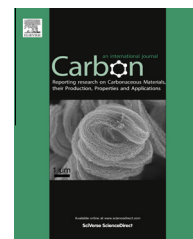


Available at www.sciencedirect.com

SciVerse ScienceDirect

journal homepage: www.elsevier.com/locate/carbon

Synthesis of graphene from asphaltene molecules adsorbed on vermiculite layers

Chenggen Xu ^a, Guoqing Ning ^{a,*}, Xiao Zhu ^a, Gang Wang ^a, Xiaofei Liu ^b, Jinsen Gao ^a, Qiang Zhang ^b, Weizhong Qian ^b, Fei Wei ^b

^a State Key Laboratory of Heavy Oil Processing, China University of Petroleum, Beijing, Changping 102249, PR China

^b Beijing Key Laboratory of Green Chemical Reaction Engineering and Technology, Department of Chemical Engineering, Tsinghua University, Beijing 100084, PR China

ARTICLE INFO

Article history:

Received 21 November 2012

Accepted 19 May 2013

Available online 13 June 2013

ABSTRACT

The strategy to regularly arrange and join the polycyclic aromatic hydrocarbons of asphalt into graphene was explored. Expanded vermiculite with a multi-layered structure was used to adsorb asphaltene molecules onto its surfaces or into its interstices, and graphene sheets with 8–10 graphene layers and a width of tens of microns were obtained by carbonization of the regularly-arranged asphalt molecules. The formation of graphene layers is ascribed to not only the regular arrangement of asphaltene molecules due to the adsorption by vermiculite layers but also the joining of the asphaltene molecules catalyzed by the Fe-containing vermiculite surfaces. By the preabsorption of melamine on vermiculite, a nitrogen-doped graphene–carbon nanotube hybrid was produced from asphalt. As anodes for Li-ion batteries, the obtained graphene materials exhibited increased capacities and rate performance as compared to the widely-used reduced graphene oxide, indicating that the asphalt-derived graphene materials have a reasonable quality.

© 2013 Elsevier Ltd. All rights reserved.

1. Introduction

Converting petroleum pitch to carbon materials by dehydrogenation is an important approach to the mass production of carbon materials and efficient usage of the fossil resource. The carbon materials prepared from petroleum pitch include active carbon [1–3], carbon foam [4,5], carbon fibers [6–8] and versatile composite or doped carbon materials [2,9–13], and have been widely used in the fields of water clearing, gas adsorption, electrodes, etc. Recently, Cheng et al. [14] have made use of the fumes from the thermal decomposition of asphalt to synthesize graphene papers on different substrates, showing the possible conversion from asphalt to graphene materials.

Up to date, it is still difficult to clearly understand the molecular structure of asphaltene, and thus less work has

been done in the structure control of the asphalt-derived carbon materials during carbonization. Asphaltene molecules have a probable molecular weight of ~750 g/mol, and the island molecular architecture dominates with one aromatic ring system per molecule [15–18], which can be regarded as fragments of graphene with functional groups. In Fig. 1, the asphalt macromolecules are illustrated as fragments of graphene, and the functional groups are omitted since some of the functional groups (such as hydroxyl groups) will be lost and some (such as branched groups) might be converted into new aromatic rings after carbonization. The structural similarity between asphalt molecules and graphene has triggered us to direct join asphalt molecules into graphene sheets. As shown in Fig. 1, on the case that the asphalt macromolecules are irregularly stacked, irregular joining of the asphalt macromolecules results in the formation of petroleum coke, which

* Corresponding author: Fax: +86 10 69724721.

E-mail address: ngq@cup.edu.cn (G. Ning).

0008-6223/\$ - see front matter © 2013 Elsevier Ltd. All rights reserved.

<http://dx.doi.org/10.1016/j.carbon.2013.05.059>

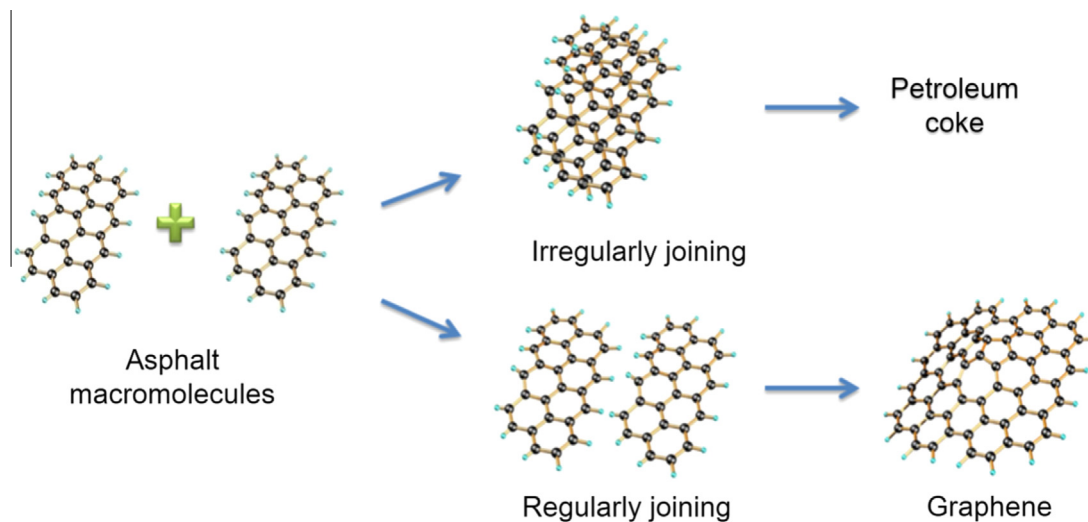


Fig. 1 – Illustration showing the carbonization mechanism of asphalt with different joining manners.

is usually composed of disordered graphite layers. If the fragments can be regularly arranged, it will be possible to obtain graphene by joining the ‘fragments of graphene’, as described in Fig. 1, which is a novel strategy for the efficient usage of heavy oil and the structure control of the asphalt-derived carbon materials. Theoretically, the direct joining of asphalt molecules is more efficient for graphene synthesis than the synthesis from pyrolyzed asphalt [14]. However, due to the complicated composition and structure of asphaltene, it is not easy to precisely arrange and regularly join the polycyclic aromatic hydrocarbons into graphene. As described by the Yen–Mullins model [17,18], with sufficient concentration in an asphaltene solution, asphaltene molecules form nanoaggregates with small aggregation numbers (<10) and with one disordered stack of aromatics. At higher concentrations, nanoaggregates form clusters, again with small aggregation numbers (<10). As a result, petroleum coke with disordered stacking of graphite layers is usually obtained after stabilization and carbonization of asphalt. By now, no work on the direct joining of asphalt molecules into graphene materials has been reported.

Here, we used expanded vermiculite with a multi-layered structure to adsorb asphaltene molecules onto surfaces or into interstices, in order to realize a regular arrangement of the asphaltene molecules. Graphene sheets with 8–10 graphene layers and a width of tens of microns were synthesized by carbonization of the regularly-arranged asphaltene molecules on the Fe-containing vermiculite layers. The formation of graphene layers is ascribed to not only the regularly arranging of asphaltene molecules due to the adsorption by vermiculite layers but also the joining of the asphaltene molecules catalyzed by the Fe-containing vermiculite surfaces. Furthermore, by the preabsorption of melamine on the vermiculite, a nitrogen-doped (N-doped) graphene-carbon nanotube (G-CNT) hybrid was produced from asphalt. The as-obtained graphene materials were tested as anodes for Li-ion batteries, and exhibited advanced capacities and rate performances as compared to the widely-used reduced graphene oxide (rGO), indi-

cating that the asphalt-derived graphene materials have a reasonable quality.

2. Experimental

Vermiculite was purchased from Lingshou, Hebei province of China. The vermiculite is composed of 38.7% O, 7.9% Mg, 10.1% Al, 25.3% Si, 4.8% K, 1.2% Ti and 12.0% Fe (weight percent), as analyzed by X-ray energy dispersive spectroscopy (EDS, Fig. S1 in Supporting Information). Asphalt was supplied by Changqing Refinery, China. Elemental analysis shows that the asphalt is composed of 88.12% C, 9.93% H, 0.56% S and 1.06% N (weight percent).

In a typical run for graphene synthesis, 1 g asphalt was dissolved in 30 mL toluene with the assistance of ultrasonication. Then, 10 g vermiculite was added into the asphalt-toluene solution and sonicated for 1 h. After that, vermiculite particles were separated from the solution by filtration, and dried in an oven overnight at 100 °C. The asphalt-adsorbed vermiculite was placed in a ceramic boat and annealed for 1 h at 700 °C in Ar flow. After the carbonization, the obtained material was washed with 10 wt.% HCl and 10 wt.% HF under stirring, followed by filtration and drying.

The synthesis process using melamine as an additive was similar to the above synthesis process, except that melamine-adsorbed vermiculite, rather than pure vermiculite, was used. The melamine-adsorbed vermiculite was obtained by adding 10 g vermiculite and 6 g melamine into 150 mL H₂O and refluxing for 1 h. Thereafter, the suspension was cooled down to room temperature, followed by filtration and drying.

The as-prepared materials were analyzed by scanning electron microscopy (SEM, Quanta 200F), transmission electron microscopy (TEM, JEM 2010 operated at 200 kV), atomic force microscopy (AFM, SPM-9600), X-ray photoelectron spectroscopy (XPS, PHI700), Raman spectroscopy (Renishaw RM2000) with the laser excitation at 633 nm and thermogravimetric analysis (TGA, Q500) measured at a heating rate of 10 °C/min in a 50 mL/min O₂ flow.

For electrochemical measurements, the graphene material was firstly calcined at 400 °C in Ar flow to remove any possible moisture or functional groups (such as hydroxyl groups) formed during the purification procedure. The working electrodes were prepared by casting a slurry containing 90 wt.% active material and 10 wt.% polyvinylidene fluoride (dispersed in *N*-methyl-2-pyrrolidone) onto a copper foil, followed by drying at 105 °C for 8 h to remove the solvent. Then the electrodes were cut into disks and dried at 110 °C for 12 h under vacuum. Li sheets were used as reference/counter electrodes, and 1 M LiPF₆ dissolved in a mixture of ethylene carbonate and dimethyl carbonate (1:1, v/v) was used as electrolyte. Galvanostatic charge–discharge cycles were tested at various current densities from 50 to 1000 mA/g between 0.01 and 3.0 V vs. Li/Li⁺. The AC impedance spectrum measurements were carried out on a CHI 660C electrochemical workstation by applying a sine wave with amplitude of 5.0 mV over the frequency range from 100 kHz to 0.01 Hz. Fitting of the impedance data was conducted by Zview (software), using “unit weighting” as the type of data weighting.

3. Results and discussion

The strategy for regularly arranging and joining asphalt molecules into graphene is shown in Fig. 2a. Asphalt solution was

adsorbed into the interstices between vermiculite layers, forming a thin coating of asphalt molecules on the surface of vermiculite layers. Graphene sheets were obtained by carbonization of the well-arranged asphalt molecules. As shown in Fig. 2b and c, the vermiculite used in this work is a russet powder with a layered structure in width of 200–500 μm. In the soaking process, we used ultrasonication to enhance the contact between the vermiculite layers and the asphalt solution. As shown in Fig. 2d, the layered structure was retained after the asphalt adsorption and carbonization. The morphology of the as-obtained graphene after the removal of vermiculite substrates was characterized by SEM and TEM. As shown in Fig. 2e and f, the graphene sheets exhibit a flat laminar morphology in width of tens of microns. High resolution TEM (HRTEM) observation (Fig. 2g) shows that orderly graphene layers can be clearly observed and the thickness of the graphene sheets is ~4 nm, corresponding to 8–10 graphene layers. AFM analysis was also performed to measure the height profile of the graphene materials (Fig. 3). The thickness of the graphene sheets measured by AFM is slightly less than 4 nm, well consistent with the HRTEM observation. It is noticeable that the surface of the graphene sheets is quite smooth, as shown in Figs. 2e, f and 3. In the TG curves of the graphene material (Fig. S2 in Supporting Information), a single weight loss peak is observed at 438.7 °C and the residue after 900 °C calcination in O₂ is 2.1 wt.%. It indicates that the

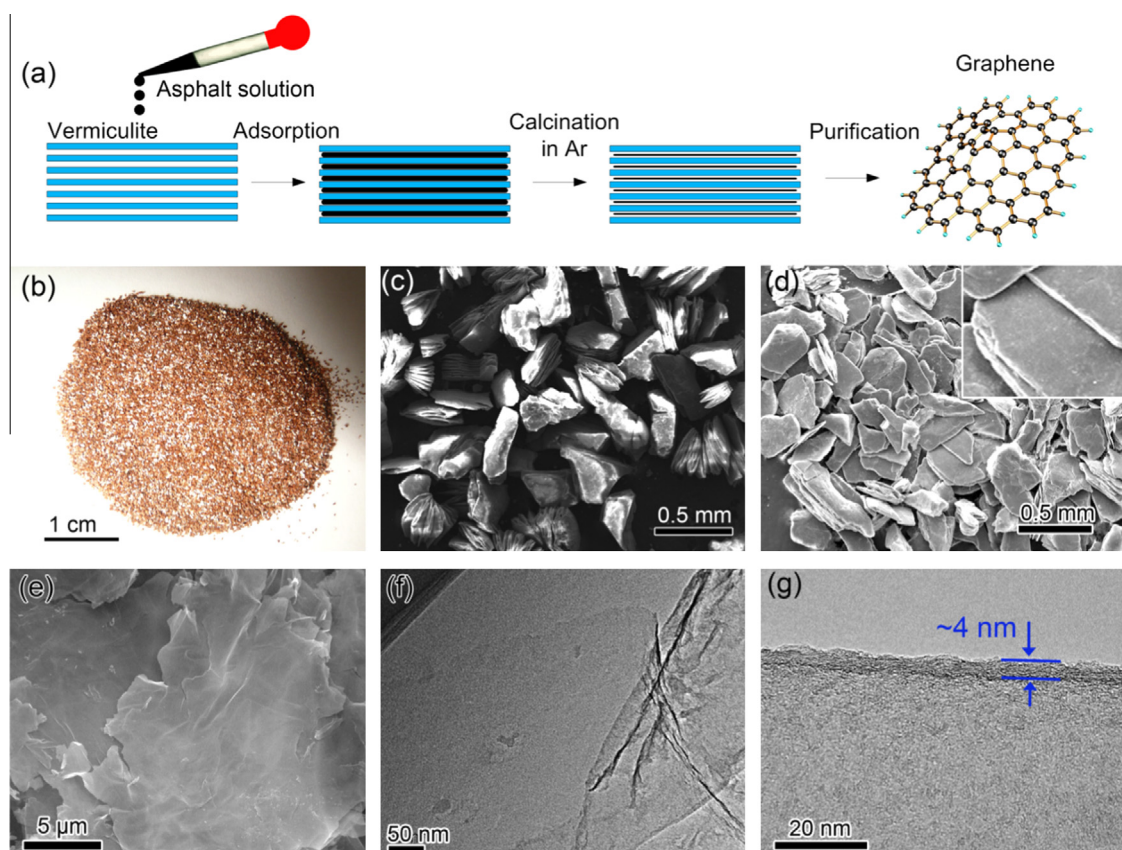


Fig. 2 – (a) Illustration of the synthesis process of graphene sheets from asphalt adsorbed by vermiculite. (b) A photo and (c) a SEM image of the vermiculite. (d) A SEM image of the vermiculite after asphalt adsorption and carbonization. The inset of (d) shows a high resolution SEM image of the material. (e) SEM and (f, g) TEM images of the as-prepared graphene sheets (after purification).

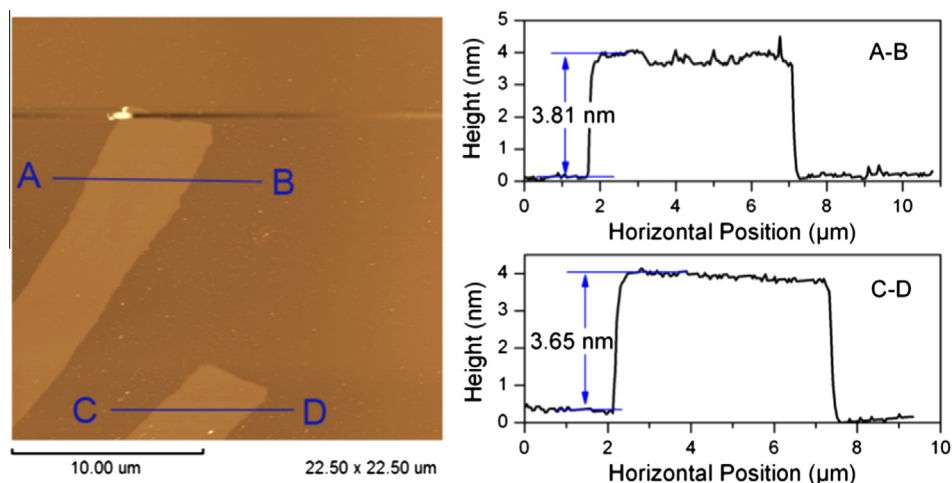


Fig. 3 – AFM image and height profiles of the asphalt-derived graphene sheets.

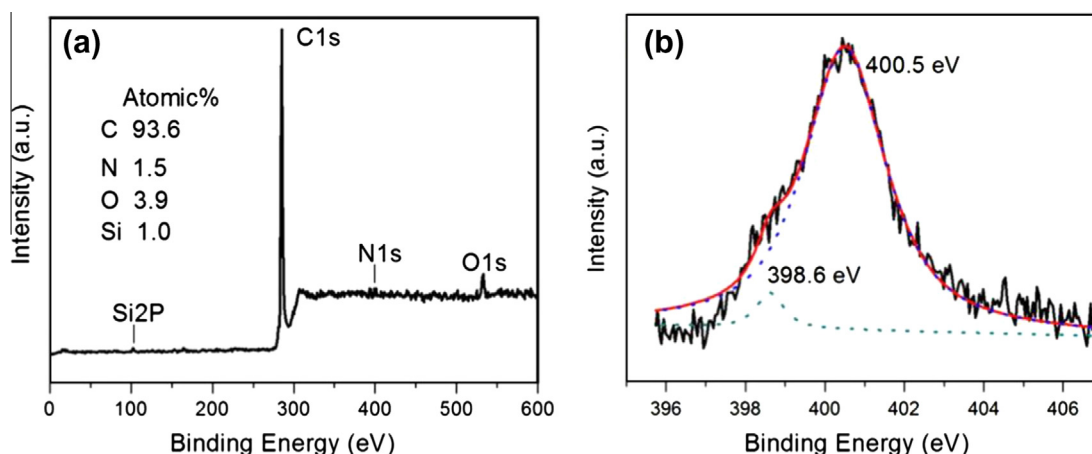


Fig. 4 – XPS curve (a) and N 1s spectrum (b) of the asphalt-derived graphene.

vermiculite substrates have been almost completely removed after the purification, leading to a high purity for the as-obtained graphene (97.9 wt.%).

The composition of the graphene material was determined by an XPS analysis (Fig. 4a). Low Si content (1.0 at.%) indicates the complete removal of the substrates by acid washing, well consistent with the TGA result. The C 1s peak centered at 284.8 eV corresponds to graphitic sp^2 C [19], and O 1s peak at ca. 533 eV is deduced to originate from the water and oxygen adsorbed on the surface of the sample [20]. Besides, N 1s peak at ca. 400 eV shows that an atomic percentage of 1.5 at.% nitrogen was detected. This is because asphalt contains a nonnegligible amount of N (1.06 wt.%), which was incorporated into the carbon structure during carbonization. The high resolution N 1s spectrum (Fig. 4b) shows that nitrogen predominantly exists in the form of pyrrolic nitrogen atoms, corresponding to the dominant peak at 400.5 eV [19]. The weak peak at 398.6 eV can be attributed to pyridinic nitrogen atoms.

The interaction between the asphalt macromolecules and the vermiculite's surfaces helps prevent the agglomeration of asphalt molecules. In a control experiment, coatings of as-

phalt macromolecules on Si substrates were prepared by spin coating. Asphalt-toluene solutions with different concentration were used to obtain coating layers with different thickness. Brittle graphite pieces in thickness of ~ 50 nm were obtained at an asphalt concentration of 0.1 g/mL (Fig. S2a, b). When using a diluted asphalt solution (0.025 g/mL), discrete spots or particles were observed on the substrate (Fig. S2c), implying that the asphalt macromolecules might have agglomerated during carbonization. The above results show that although joining asphalt macromolecules into graphene is theoretically feasible, it is still difficult to realize such a process by making an asphalt coating on Si substrates. On the case that asphalt is adsorbed into the interlayer spaces of vermiculite, the good adsorbability of the vermiculite multilayers and the confinement effect might have resulted in an orderly stacking of asphalt molecules and prevented their agglomeration during carbonization. The existence of Fe species (12 wt.%) in vermiculite may also play an important role in the formation of graphene sheets, which will be discussed later.

Furthermore, we used melamine as nitrogen source to produce N-doped graphene material [21]. Interestingly, a N-

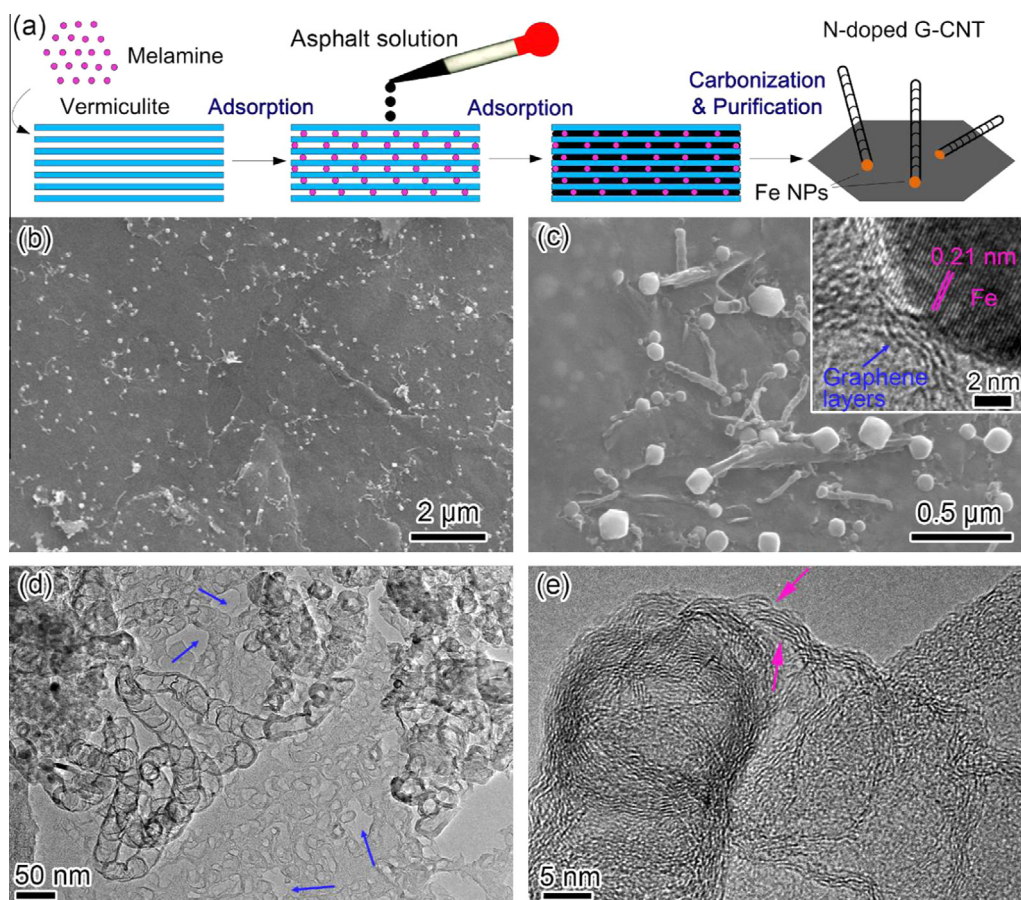


Fig. 5 – (a) Illustration showing the synthesis process of the N-doped G-CNT hybrid using vermiculite with asphalt and melamine. (b and c) SEM images of the G-CNT hybrid formed on vermiculite layers before purification. The inset of (c) shows the HRTEM image of a Fe nanoparticle on the root of a CNT. (d) TEM images of the G-CNT hybrid after purification. (e) HRTEM image of a CNT in the G-CNT hybrid.

doped G-CNT hybrid was actually obtained after adding malamine. The N-doping process is illustrated in Fig. 5a. First, melamine and asphalt are adsorbed into the interlayer spaces of vermiculite in turn. During the carbonization process, pyrolysis of melamine will lead to the formation of NH_3 [22], which can reduce the Fe species in vermiculite to form Fe nanoparticles (NPs). As a result, both graphene sheets and CNTs are grown on the vermiculite layers, thus forming a N-doped G-CNT hybrid. As shown in Fig. 5b and c, evenly distributed NPs and CNTs can be found on the surface of the material after carbonization (before removal of vermiculite). Some NPs are on the root of the CNTs, indicating that the growth of CNTs has been catalyzed by the NPs. As measured from the HRTEM image of the NPs (the inset of Fig. 5c), the lattice spacing (0.21 nm) matches well with the (111) spacing of γ -Fe, confirming that the catalytic NPs are Fe species. TEM observation (Fig. 5d) shows that the CNTs have a bambo-like morphology, which is typical for N-doped CNTs. Broken sites of graphene layers can be clearly observed in Fig. 5e (for example, the sites indicated by the arrows), implying that the N-doping might have introduced many defects into the G-CNT hybrid [23–25]. XPS measurement shows that the nitrogen content is 10.7 at.% for the N-doped G-CNT hybrid (Fig. 6a), much larger than that of the undoped graphene

(1.5 at.%). The N 1s peak of the N-doped G-CNT (Fig. 6b) splits into two components centered at 398.4 and 400.2 eV, representing pyridinic and pyrrolic nitrogen atoms [26,27], respectively. As compared to the asphalt-derived graphene (Fig. 4b), the peak at 398.4 eV is much stronger for the N-doped G-CNT, indicating that the N-doping by melamine has significantly contributed to the formation of pyridinic nitrogen atoms.

In the TEM images of the N-doped G-CNT (Fig. 5d), both nanopores (indicated by arrows) and ultra-short CNTs can be found. The ultra-short CNTs were formed probably due to the limited amount of asphalt coating, which terminated further growth of the CNTs. The formation of nanopores might indicate that the existence of Fe species may be a key factor to the formation of graphene layers since the Fe content in vermiculite layers is as high as 12 wt.%. Once the Fe species are reduced into Fe NPs, there exists some Fe-free area on the vermiculite layers, which may lead to the formation of nanopores in graphene sheets. Without melamine, no Fe NPs are found in the as-prepared materials (inset of Fig. 2d), showing that the agglomeration of Fe species has been avoided. As a result, the evenly distributed Fe species have catalyzed the joining of asphalt molecules into graphene sheets with well-ordered graphene layers. Raman spectra of the graphene and the N-doped G-CNT hybrid are presented

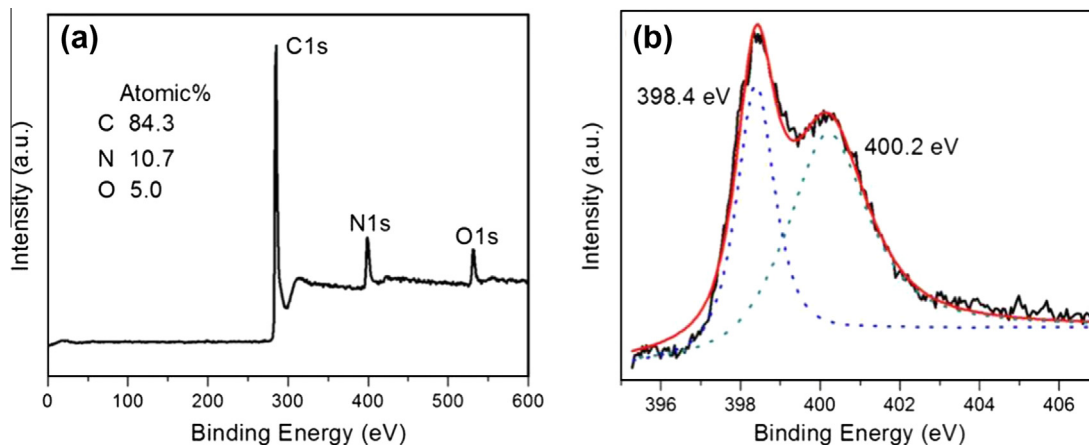


Fig. 6 – XPS curve (a) and N1s spectrum (b) of the N-doped G-CNT.

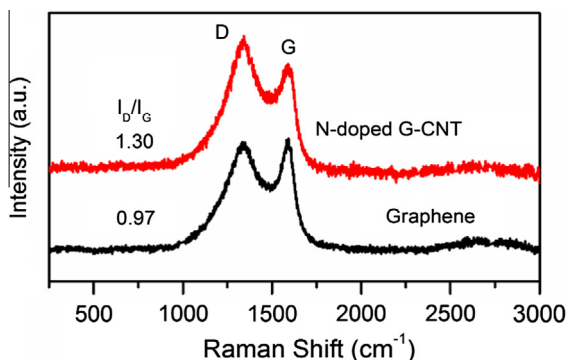


Fig. 7 – Raman spectra of the graphene and the N-doped G-CNT hybrid (normalized by the G bands).

in Fig. 7. The D band to G band ratio (I_D/I_G) of the N-doped G-CNT hybrid (1.30) is obviously higher than that of the graphene (0.96), indicating that there exist more defects or disorders in the N-doped G-CNT hybrid. The defects might be attributed to nitrogen intercalation [28] and the existence of a large amount of pores and edges in the N-doped material.

The two asphalt-derived graphene materials were used as anode materials for Li-ion batteries. Lithiation/delithiation curves of the graphene and the N-doped G-CNT are shown in Fig. 8. In the first lithiation process, a voltage plateau at about 0.7 V is observed, which can be assigned to the decomposition of electrolyte and the formation of the solid electrolyte interphase (SEI) film [29]. The first lithiation and delithiation capacities for the graphene electrode are 1071 and 692 mAh/g, higher than the N-doped G-CNT electrode (853 and 625 mAh/g). But the latter possesses a higher coulombic efficiency in the first cycle (73% for the N-doped G-CNT and 65% for the graphene). More importantly, after the first two cycles at 50 mA/g, the reversible capacity of the N-doped G-CNT overtakes that of the graphene and maintains the lead at higher current densities (Fig. 9a). At the current density of 1000 mA/g, the N-doped G-CNT electrode delivers a stable capacity of 380 mAh/g, which is 50% higher than the value for the graphene electrode (~250 mAh/g). After the test of rate performance, the cells were cycled for another

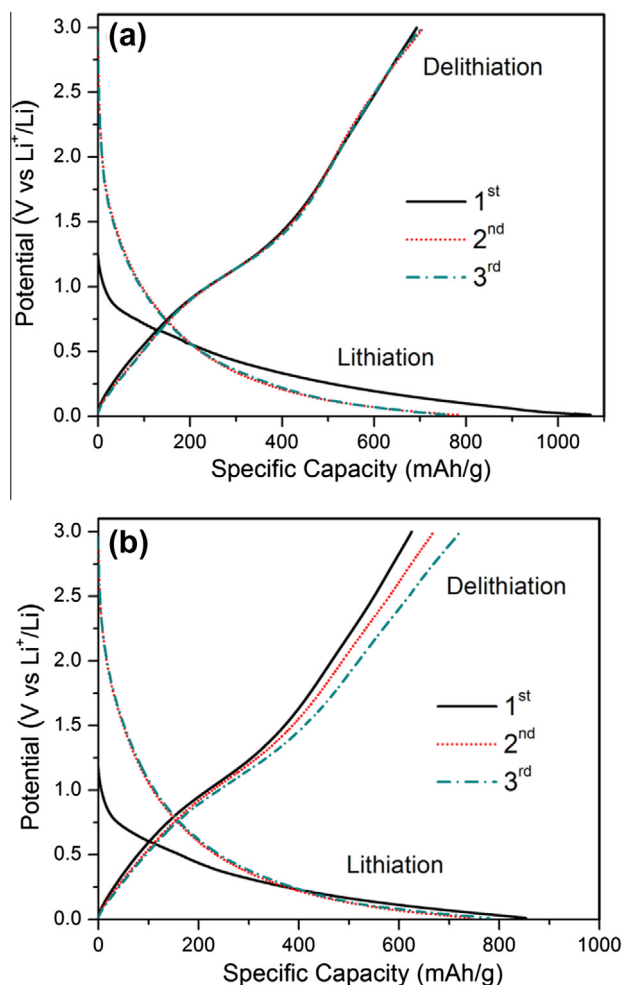


Fig. 8 – Lithiation/delithiation curves of the graphene (a) and the N-doped G-CNT (b).

90 cycles at 150 mA/g. As illustrated in Fig. 9b, both the two materials exhibit good cycling stability. The average capacity for the N-doped G-CNT electrode is 606 mAh/g at 150 mA/g, obviously larger than that for the asphalt-derived graphene (479 mAh/g at 150 mA/g).

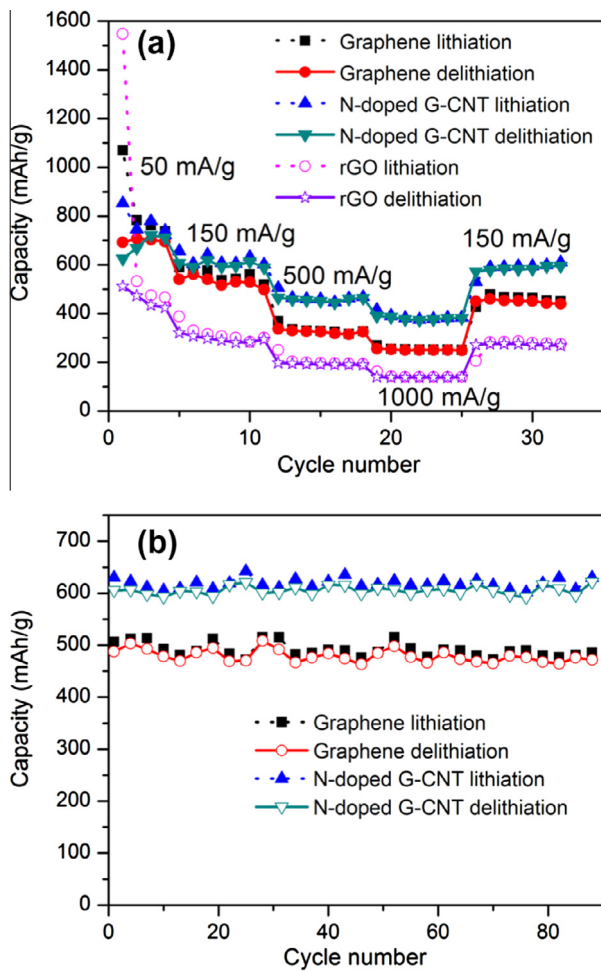


Fig. 9 – Rate capability (a) and cycling performance at 150 mA/g (b) of the graphene and the N-doped G-CNT hybrid.

Two main reasons are proposed to explain the superior reversible capacity of the N-doped G-CNT electrode as compared to the graphene electrode. Firstly, N-doping introduces a lot of defects into graphene layers, which is beneficial to Li insertion and storage [30]. The pyridinic nitrogen atoms in the N-doped G-CNT can also contribute to the capacity improvement [26]. Secondly, the three-dimensional composite structure with nanopores of the N-doped G-CNT owns expanded inner space, which avoids the agglomeration of graphene layers, favors lithium diffusion and transfer, and heightens the lithium storage capacity. Nyquist complex plane impedance plots of the graphene and the N-doped G-CNT electrodes are presented in Fig. 10. The equilibrium potentials of the impedance measurements were 2–3 V, e.g., 2.77 and 2.17 V for the N-doped G-CNT electrode before and after the rate tests. The equivalent circuit shown in Fig. 10a was used to fit the impedance data for the electrodes before and after the test of rate capability. In the equivalent circuit, R_e represents the resistance of the electrolyte, R_f and CPE_1 represent the resistance and the capacitance (expressed by a constant phase element) of SEI films, R_{ct} and CPE_2 correspond to the charge-transfer resistance and the double-layer capacitance (expressed by a constant phase element), and Z_w is the War-

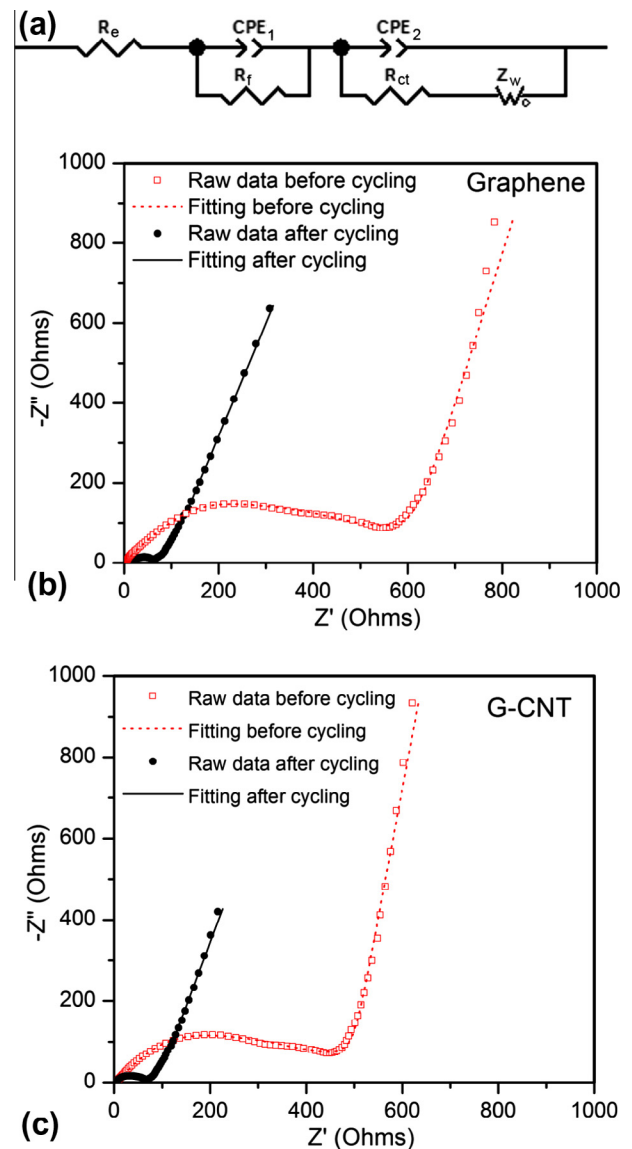


Fig. 10 – Equivalent circuit (a) and Nyquist plots for the asphalt-derived graphene (b) and the N-doped G-CNT (c).

Table 1 – The calculated values of R_e , R_f and R_{ct} through fitting of the experimental impedance spectra.

(Ω)	Graphene		N-doped G-CNT	
	Before	After	Before	After
R_e	0.6	8.2	3.7	5.2
R_f	41.4	29.1	62.4	42.3
R_{ct}	492.5	11.7	382.7	9.7

burg impedance related to the diffusion of lithium ions through the bulk of the electrode. The calculated values of R_e , R_f and R_{ct} through fitting of the experimental impedance spectra are summarized in Table 1. The SEI film resistance (R_f) and the charge-transfer resistance (R_{ct}) are obviously reduced after the rate tests as compared to those before cycling, indicating that much better contact between electrolyte and electrode materials has been realized after the cycling. After

the rate test, the resistance of the electrolyte (R_e) and the charge-transfer resistance (R_{ct}) for the N-doped G–CNT electrode (5.2 and 9.7 Ω) are lower than those for the graphene electrode (8.2 and 11.7 Ω). The porous structure of the N-doped G–CNT can increase the electrolyte contact area and the structure defects induced by N-doping might reduce the energy barrier of Li intercalation into graphene and CNTs [28], which is propitious to reduce the resistance for Li ion diffusion. The SEI film resistance (R_f) for the N-doped G–CNT (42.3 Ω) is higher than that for the graphene (29.1 Ω), indicating that thicker SEI films have been formed on the N-doped G–CNT probably due to the larger contact area between electrolyte and the porous G–CNT hybrid.

Compared to rGO, the graphene derived from asphalt exhibits advanced electrode performance. As shown in Fig. 9a, the average capacity for the asphalt-derived graphene is 699.4 mAh/g at 50 mA/g (corresponding to the current density of 0.2 mA/cm²), higher than the capacity for rGO measured in our lab (468.4 mAh/g on average at 50 mA/g) and reported in most literatures (<600 mAh/g at 0.2 mA/cm² [29], 540 mAh/g at 50 mA/g [31] and 550 mAh/g at a slightly lower current density of 42 mA/g [19]). Although the capacity for the asphalt-derived graphene is lower than the rGO reported by Lian et al. (up to 1264 mAh/g at 100 mA/g) [32], the cycling stability of the asphalt-derived graphene is much better than the rGO (67% capacity remained after 40 cycles). Therefore, it can be concluded that the electrode performance of the asphalt-derived graphene is at least comparable to the widely-applied rGO materials. The high capacity of the asphalt-derived graphene can be ascribed to the absence of oxygen-containing functional groups and the N-doping as shown by the XPS measurement (Fig. 4). It has been reported that the removal of oxygen-containing functional groups can improve the conductivity of graphene [33]. In order to test the conductivity of the asphalt-derived graphene, graphene papers were fabricated by flow-directed filtration of a graphene-containing suspension as reported in our recent publication [34]. The conductivity of the as-prepared graphene paper, measured by a four-wire setup, is 3327 ± 22 S/m, much higher than that of the rGO paper reported by Compton et al. (1500 ± 200 S/m) [35]. Therefore, the good conductivity of the asphalt-derived graphene might also be an important factor that leads to its advanced electrode performance.

4. Conclusions

Regularly arranging and joining asphalt molecules into graphene was realized by adsorbing asphalt molecules onto the surface of expanded vermiculite layers. The formation of graphene layers is ascribed to not only the regular arrangement of asphaltene molecules due to the adsorption by vermiculite layers but also the joining of the asphaltene molecules catalyzed by the Fe-containing vermiculite surfaces. By adding melamine, the N-doped G–CNT hybrid with a porous structure was obtained with a N content as high as 10.7 at.%. As anode materials in Li-ion batteries, the asphalt-derived graphene materials exhibited larger reversible capacity than rGO. Compared with the as-prepared graphene, the N-doped G–CNT showed advanced electrode performance due to N-doping and its porous structure. Our work demon-

strated a novel approach for graphene synthesis by regularly arranging and joining asphaltene molecules, and realized the production of high performance anode materials through high-efficient utilization of asphalt.

Acknowledgement

This work was supported by the National Natural Science Foundation of China (No. 21206191) and the Science Foundation of China University of Petroleum, Beijing (QD-2010-03).

Appendix A. Supplementary data

Supplementary data associated with this article can be found, in the online version, at <http://dx.doi.org/10.1016/j.carbon.2013.05.059>.

REFERENCES

- [1] Daguerre E, Guillot A, Py X. Microporosity of activated carbons produced from heat-treated and fractionated pitches. *Carbon* 2000;38(1):59–64.
- [2] Park JG, Yun NG, Park YB, Liang R, Lumata L, Brooks JS, et al. Single-walled carbon nanotube buckypaper and mesophase pitch carbon/carbon composites. *Carbon* 2010;48(15):4276–82.
- [3] Lozano-Castello D, Alcaniz-Monge J, Cazorla-Amorós D, Linares-Solano A, Zhu W, Kapteijn F, et al. Adsorption properties of carbon molecular sieves prepared from an activated carbon by pitch pyrolysis. *Carbon* 2005;43(8):1643–51.
- [4] Klett J, Hardy R, Romine E, Walls C, Burchell T. High-thermal-conductivity, mesophase-pitch-derived carbon foams: effect of precursor on structure and properties. *Carbon* 2000;38(7):953–73.
- [5] Wang M, Wang C, Chen M, Li T, Hu Z. Bubble growth in the preparation of mesophase-pitch-based carbon foams. *New Carbon Mater* 2009;24(1):61–6.
- [6] Park S-J, Jang Y-S, Shim J-W, Ryu S-K. Studies on pore structures and surface functional groups of pitch-based activated carbon fibers. *J Colloid Interface Sci* 2003;260(2):259–64.
- [7] Derbyshire F, Andrews R, Jacques D, Jagtoyen M, Kimber G, Rantell T. Synthesis of isotropic carbon fibers and activated carbon fibers from pitch precursors. *Fuel* 2001;80(3):345–56.
- [8] Cho T, Lee YS, Rao R, Rao AM, Edie DD, Ogale AA. Structure of carbon fiber obtained from nanotube-reinforced mesophase pitch. *Carbon* 2003;41(7):1419–24.
- [9] Blanco C, Santamaría R, Bermejo J, Menéndez R. Pitch-based carbon composites with granular reinforcements for frictional applications. *Carbon* 2000;38(7):1043–51.
- [10] Tamai H, Kataoka Y, Nishiyama F, Yasuda H. Characteristics and catalytic activity of carbons obtained from pitch containing noble metal complexes. *Carbon* 2000;38(6):899–906.
- [11] Tamai H, Matsuoka S, Ishihara M, Yasuda H. New carbon materials from pitch containing organotin compounds for anode of lithium ion batteries. *Carbon* 2001;39(10):1515–23.
- [12] Bulusheva LG, Okotrub AV, Fedoseeva YV, Shlyakhova EV, Huo J, Song H, et al. Electronic state of carbon in nanostructured composites produced by co-carbonization of aromatic heavy oil and ferrocene. *Mater Chem Phys* 2010;122(1):146–50.
- [13] Fathollahi B, Chau PC, White JL. Injection and stabilization of mesophase pitch in the fabrication of carbon–carbon

- composites. Part I. Injection process. *Carbon* 2005;43(1):125–33.
- [14] Cheng IF, Xie Y, Allen Gonzales R, Brejna PR, Sundararajan JP, Fouetio Kengne BA, et al. Synthesis of graphene paper from pyrolyzed asphalt. *Carbon* 2011;49(8):2852–61.
- [15] Murgich J, Rodríguez J, Aray Y. Molecular recognition and molecular mechanics of micelles of some model asphaltenes and resins. *Energy Fuel* 1996;10(1):68–76.
- [16] Merdrignac I, Espinat D. Physicochemical characterization of petroleum fractions: the state of the art. *Oil Gas Sci Technol* 2007;62(1):7–32.
- [17] Mullins OC, Sabbah H, Eyssautier J, Pomerantz AE, Barré L, Andrews AB, et al. Advances in asphaltene science and the Yen–Mullins Model. *Energy Fuel* 2012;26(7):3986–4003.
- [18] Mullins OC. The modified Yen Model. *Energy Fuel* 2010;24(4):2179–207.
- [19] Wang H, Zhang C, Liu Z, Wang L, Han P, Xu H, et al. Nitrogen-doped graphene nanosheets with excellent lithium storage properties. *J Mater Chem* 2011;21(14):5430–4.
- [20] Wei DC, Liu YQ, Wang Y, Zhang HL, Huang LP, Yu G. Synthesis of N-Doped graphene by chemical vapor deposition and its electrical properties. *Nano Lett* 2009;9(5):1752–8.
- [21] Sheng ZH, Shao L, Chen JJ, Bao WJ, Wang FB, Xia XH. Catalyst-free synthesis of nitrogen-doped graphene via thermal annealing graphite oxide with melamine and its excellent electrocatalysis. *ACS Nano* 2011;5(6):4350–8.
- [22] Li X, Zhang J, Shen L, Ma Y, Lei W, Cui Q, et al. Preparation and characterization of graphitic carbon nitride through pyrolysis of melamine. *Appl Phys A* 2008;94(2):387–92.
- [23] Guo BD, Liu QA, Chen ED, Zhu HW, Fang LA, Gong JR. Controllable N-doping of graphene. *Nano Lett* 2010;10(12):4975–80.
- [24] Chun K-Y, Lee HS, Lee CJ. Nitrogen doping effects on the structure behavior and the field emission performance of double-walled carbon nanotubes. *Carbon* 2009;47(1):169–77.
- [25] Ayala P, Arenal R, Ruemmel M, Rubio A, Pichler T. The doping of carbon nanotubes with nitrogen and their potential applications. *Carbon* 2010;48(3):575–86.
- [26] Reddy ALM, Srivastava A, Gowda SR, Gullapalli H, Dubey M, Ajayan PM. Synthesis of nitrogen-doped graphene films for lithium battery application. *ACS Nano* 2010;4(11):6337–42.
- [27] Qu LT, Liu Y, Baek JB, Dai LM. Nitrogen-doped graphene as efficient metal-free electrocatalyst for oxygen reduction in fuel cells. *ACS Nano* 2010;4(3):1321–6.
- [28] Bulusheva LG, Okotrub AV, Kurenaya AG, Zhang H, Zhang H, Chen X, et al. Electrochemical properties of nitrogen-doped carbon nanotube anode in Li-ion batteries. *Carbon* 2011;49(12):4013–23.
- [29] Guo P, Song H, Chen X. Electrochemical performance of graphene nanosheets as anode material for lithium-ion batteries. *Electrochem Commun* 2009;11(6):1320–4.
- [30] Shin WH, Jeong HM, Kim BG, Kang JK, Choi JW. Nitrogen-doped multiwall carbon nanotubes for lithium storage with extremely high capacity. *Nano Lett* 2012;11:8–10.
- [31] Yoo E, Kim J, Hosono E, Zhou H-S, Kudo T, Honma I. Large reversible Li storage of graphene nanosheet families for use in rechargeable lithium ion batteries. *Nano Lett* 2008;8(8):2277–82.
- [32] Lian P, Zhu X, Liang S, Li Z, Yang W, Wang H. Large reversible capacity of high quality graphene sheets as an anode material for lithium-ion batteries. *Electrochim Acta* 2010;55(12):3909–14.
- [33] Chen H, Muller MB, Gilmore KJ, Wallace GG, Li D. Mechanically strong, electrically conductive, and biocompatible graphene paper. *Adv Mater* 2008;20(18):3557–61.
- [34] Ning G, Xu C, Cao Y, Zhu X, Jiang Z, Fan Z, et al. Chemical vapor deposition derived flexible graphene paper and its application as high performance anodes for lithium rechargeable batteries. *J Mater Chem A* 2013;1(2):408–14.
- [35] Compton OC, Dikin DA, Putz KW, Brinson LC, Nguyen ST. Electrically conductive “alkylated” graphene paper via chemical reduction of amine-functionalized graphene oxide paper. *Adv Mater* 2010;22(8):892–6.